

Unraveling the role of adapting risk perception during the COVID-19 pandemic in Europe

Bastian Heinlein^a, Manlio De Domenico^{b,c,d,*}

^a Friedrich-Alexander-Universität Erlangen-Nürnberg, Germany

^b Department of Physics and Astronomy "Galileo Galilei", University of Padua, Via F. Marzolo 8, 315126 Padova, Italy

^c Padua Center for Network Medicine, University of Padua, Via F. Marzolo 8, 315126 Padova, Italy

^d Istituto Nazionale di Fisica Nucleare, Sez. Padova, Italy

Abstract

During the COVID-19 pandemic, the behavioral response to reported case numbers changed drastically over time. While a few dozen cases were enough to trigger government-induced and voluntary contact reduction in early 2020, less than a year later, much higher case numbers were required to induce behavioral change. Little attention has been paid to understand, and mathematically model, this effect of decreasing risk perception over longer time-scales. Here, first we show that weighing the number of cases with a time-varying factor of the form t^a , $a < 0$ explains real-world mobility patterns from several European countries during 2020 when introduced into a very simple behavior model. Subsequently, we couple our behavior model with an SIR epidemic model. Remarkably, decreasing risk perception can produce complex dynamics, including multiple waves of infection. We find two regimes for the total number of infected individuals that are explained by the interplay of initial attention and the rate of attention decrease. Our results show that including adaptation into non-equilibrium models is necessary to understand behavior change over long time scales and the emergence of non-trivial infection dynamics.

Keywords: COVID-19, Epidemic Spreading, Ordinary Differential Equation, Population Behavior

1. Introduction

The behavioral response to the COVID-19 pandemic changed considerably over time. While relatively few reported cases were enough to trigger massive mobility reductions in March 2020, a much higher reported prevalence was necessary to elicit a similar response at the end of the year. Now, adherence to recommended non-pharmaceutical interventions (NPIs) dropped dramatically since the World Health Organization (WHO) declared that COVID-19 no longer poses an health emergency of international concern [1]. Yet, only a few attempts have been made to explain these drastic changes of the behavioral response.

One reason for this might be the lack of longitudinal data about behavior change. Even though some studies collected survey data over longer periods [2, 3, 4, 5], they miss relevant phases of the pandemic, especially the period when the first cases were reported. Furthermore, the used questionnaires typically changed over time, making analyses more difficult.

To overcome this limitation we propose to interpret mobility data as a proxy for behavior change. In contrast

to surveys, mobility data is continuously captured from smartphones and wearable devices in most countries. Aggregate data about mobility reduction during the COVID-19 pandemic has been readily provided, e.g., by Google [6] and Apple [7]. Conveniently, these data are not subject to biases typical of self-reported answers in a survey. Furthermore, mobility reflects actual behavior whereas surveys are often concerned with the intent of behavior change, even though it is well known that the intent to change behavior does not fully predict actual behavior change [8].

Not only is mobility data widely available, but also already a tool in modern epidemiology. The structure of air transportation networks has been used to predict the spread of pathogens between countries already more than a decade ago [9]. More recently, within-country mobility that is measured, e.g., using mobile phones, has become a common tool during the COVID-19 pandemic motivated by its potential to explain or predict infection dynamics [10, 11], even though the relationship between mobility and infection dynamics is non-trivial on longer time scales [12, 13].

Furthermore, some studies already analyzed possible causes of mobility change [14, 15, 16, 17] and its evolution over time [18]. However, these studies typically did not provide mechanistic models for mobility change but rather analyzed if there are relations at all, e.g., between government regulations (GRs) and mobility reduction.

*Corresponding author

Email addresses: bastian.heinlein@fau.de (Bastian Heinlein), manlio.dedomenico@unipd.it (Manlio De Domenico)

On the other hand, there is also a lot of work that incorporates behavior change as a response to infection dynamics into epidemiological models [19]. This has been often done in a more theoretical fashion [20, 21, 22, 23, 24] where resulting infection dynamics are analyzed. Often, these models are not validated with real-world data, again probably due to a lack of behavior data. Thus, some authors instead validated their models with reported case numbers [25, 26]. However, as argued in [27], this approach suffers from a generally time-varying under-reporting factor and neglects the fact that infection dynamics are not solely influenced by a single protection behavior (PB), but also, e.g., by other NPIs, vaccinations [28], and seasonality [29].

A few exceptions exist, where detailed behavior models were proposed and also validated, e.g., in [27], a mathematical interpretation of the Health Belief Model (HBM) [30] was developed and validated with data about mask-wearing during the 2003 SARS epidemic in Hong Kong. The effect of risk-perception on the 2009 H1N1 influenza dynamics was investigated in [31]. There, an extended susceptible-infectious-removed (SIR) model was developed and fitted not only to epidemiological data but also the behavior component compared to data about purchases of antivirals. The TELL ME-project is a cautionary tale about the necessity of validating behavioral models. Even though experts considered its results "realistic", a comparison of its outputs to survey data revealed stark differences to empirical results [32].

In this paper, we extend the literature by introducing an ordinary differential equation (ODE)-based behavioral model that is validated with aggregate mobility data from nine European countries between March 01st and December 31st, 2020. This model can reproduce the key trends of the mobility change in this period despite large inter-country differences. The key element is a time-dependent risk perception.

We couple our behavioral model to an SIR model and demonstrate that this can lead to complex infection dynamics, including multiple peaks of infection that resemble realistic infection patterns. Through a comprehensive analytical treatment, we identify two distinct regimes for the final number of susceptibles depending on the behavioral and epidemiological parameters. We provide a theoretical explanation for the emergence of these regimes.

The remainder of this paper is organized as follows: In Sec. 2, we explain the psychological motivations behind our model and introduce its mathematical formulation. In Sec. 3, we validate this behavioral model with mobility data before coupling it with an SIR model in Sec. 4. Finally, we provide an analysis of the resulting model dynamics in Sec. 5 and summarize our main findings and provide an outlook about potential extensions in Sec. 6.

2. Behavior Model: Introduction

We devise a simple, psychologically motivated model with time-variant weighing of the reported number of cases.

2.1. Motivation

Similar to Durham et al. [27], we make use of the HBM as foundation for our behavior model. The adoption of PB is assumed to depend on the four factors (1) perceived likelihood of infection (*susceptibility*), (2) perceived likelihood of severe disease if infected (*severity*), (3) perceived benefits of, and (4) perceived barriers against adopting the corresponding behavior.

Empirical psychological research supports this theoretical framework, i.e., that higher perceived susceptibility, higher perceived severity, and higher perceived PB efficacy are relevant predictors of higher PB adoption [33].

A key insight about the HBM is the emphasis on the *perception* of these factors. So, even if the actual severity of a disease typically stays constant over time¹, the perceived severity can change. The perception, and in turn adoption of PB, can change, e.g., due to media consumption [34, 35], (maladaptive) coping mechanisms [36], infodemics, or simply the fact that evidence about a novel disease has to be gathered over time.

Similarly, the perceived likelihood of infection might also differ from the actual likelihood of infection. One example is having a time-varying under-reporting factor. However, even the reported number of cases can be interpreted differently as time progresses, simply because humans might get used to higher infection levels and therefore reduce their reaction to them. Over time, individuals might notice that they actually have not got infected and therefore higher reported case numbers are necessary to trigger the adoption of PB.

Furthermore, the perceived efficacy of PB might decrease over time as shown in [37]. There, the authors found a high perceived efficacy early in the COVID-19 pandemic and argued that these high expectations might not have been met, causing a decrease of the perceived efficacy later on.

Finally, the perceived barriers can reduce the adoption of PB, e.g., the higher the social, economic, or emotional cost associated with a certain PB, the larger the tendency to stop adopting it.

2.2. Model Definition

We propose a mathematical model for the evolution of the fraction of individuals adopting PB. Specifically, we argue that individuals either adopt PB or not.

¹Of course, the introduction of vaccines or increasing population immunity can reduce the actual severity. However, we focus on a time-period where these factors can be neglected.

In order to operationalize the insights from Section 2.1, we propose the ODE

$$\frac{dp(t)}{dt} = [f_0 \cdot (t+1)^a \cdot c(t)] \cdot [1 - p(t)] + g_0 \cdot p(t), \quad (1)$$

where $f_0, g_0 \geq 0$ and $a \leq 0$ are the model parameters. $p(t) \in [0, 1]$ and $c(t)$ denote the fraction of the population that adopts PB and the reported number of cases on day t , respectively.

In this model, f_0 governs how "sensitive" the population is to the reported number of cases. The term $(t+1)^a$ is the time-varying factor that weighs $c(t)$. For $a < 0$, the rate to adopt PB decreases over time for a fixed value of $c(t)$.

To interpret this expression, we first note that the uptake of PB requires that one feels *susceptible* to a *severe* disease and assumes that the respective PB is *effective* in reducing their risk of infection. Thus, a decrease of any of these factors reduces the adoption rate of PB. Hence, the time-variant factor could be seen as a decrease of a single factor or as a decrease of several factors. For example, one could argue that the perceived severity and efficacy stay constant over time, but for a given reported prevalence, the perceived susceptibility reduces. Or, the perceived susceptibility could stay constant, but both the perceived severity and PB efficacy go down.

Finally, g_0 governs the tendency to stop adopting PB and is related to the (perceived) cost associated with PB².

3. Behavior Model: Validation

In this section, we show that our behavior model is able to explain key trends in real-world mobility data from various European countries, despite its very low complexity and the long time-frame under consideration.

3.1. Motivation

While many epidemic models incorporating a behavioral component haven been proposed, only few of them have been validated with real-world data. As explained in the introduction, mobility data can be used as a proxy for behavior change to alleviate the issue of not being able to validate behavior models due to a lack of survey data over the relevant time-frames.

3.2. Data Sources and Fitting Procedure

Google provided aggregate data about the mobility change in countries during the COVID-19 pandemic. Specifically, for certain categories of mobility, in our case

retail and recreation, the relative mobility change defined as

$$\Delta_m^{\text{obs}}(t) = \frac{m^{\text{obs}}(t)}{m^{\text{base}}(t)} - 1. \quad (2)$$

is provided on a daily level. Here, $m^{\text{obs}}(t)$ and $m^{\text{base}}(t)$ denote the observed amount of mobility on day t and the baseline amount of mobility, meaning the expected mobility in absence of any behavior change, on day t , respectively. Thus, a mobility reduction is indicated by negative values of $\Delta_m^{\text{obs}}(t)$.

For simplicity, we assume that an individual either is mobile or is not, i.e., we would expect no mobility at all if $p(t) = 1$, i.e., if everybody adopts PB. Therefore, we can calibrate the model parameters f_0 , a , and g_0 by minimizing

$$\text{RMSE} = \sqrt{\frac{1}{t_{\text{obs}}} \sum_{t=0}^{t_{\text{obs}}-1} (p(t) - \text{ReLU}(-\Delta_m^{\text{obs}}(t)))^2}, \quad (3)$$

where t_{obs} denotes the number of considered days and $\text{ReLU}(\cdot)$ the rectified linear unit function.

For a detailed description of the used data and fitting procedure, we refer to Appendix A.

3.3. Results

In Fig. 1, we show the observed mobility reduction $-\Delta_m^{\text{obs}}(t)$ in nine European countries from March 01st to Dec. 31st 2020, the fraction of individuals adopting PB $p(t)$, and the normalized reported number of cases $c(t)$ in blue, green, and red, respectively. The inferred parameters are reported in Appendix B, where we also show the parameters and fitting errors for the alternative end dates of Nov. 30th 2020 and Jan. 31st 2021, respectively.

As a first observation we note the large inter-country differences of both $c(t)$ and $\Delta_m^{\text{obs}}(t)$. Yet, some general patterns emerge. In all countries, there is a large mobility reduction early on in the pandemic. Then, over time the mobility level goes back to normal. Typically, only when a pronounced second wave of infections occurs, mobility is reduced again. However, the height and duration of mobility reductions differ considerably and also whether the mobility reduction is larger during the first or second wave of infections.

Despite these large variations, the mobility reduction is well captured by our model in all countries. Especially, during the first wave of infections, the mobility patterns are almost exactly reproduced. During the second wave, the general trend of having a considerable mobility reduction is again captured. However, some specifics are not described by the model.

For example, the mobility in Germany is additionally reduced around $t = 290$ despite an earlier reduction around $t = 260$. $p(t)$ remedies this by assuming a higher initial mobility reduction and only a slight subsequent increase in PB. Indeed, it is not surprising that our model cannot reproduce these exact mobility patterns: The second mobility reduction happened due to the introduction of

²Note that one could also argue that this cost increases over time. Then, similar model dynamics would be expected as when assuming decreasing perceived susceptibility/severity. However, a - generally unbounded - increasing function poses numerical issues and is thus not considered in this paper.

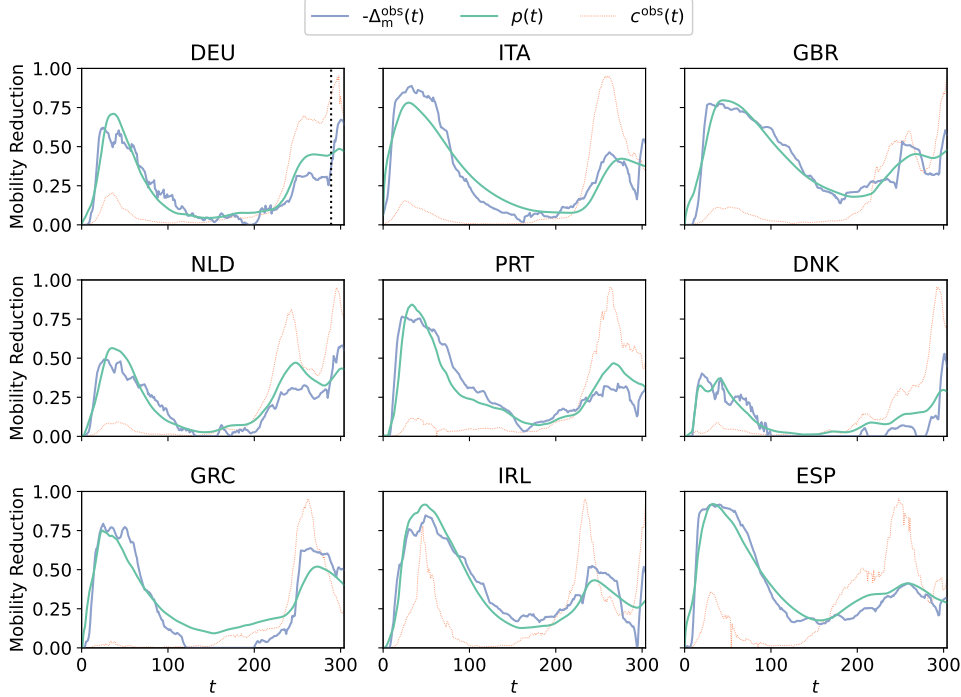


Figure 1: Observed mobility reduction (blue), corresponding model fits (green) and normalized smoothed number of reported cases (red) for nine European countries between Mar. 1st, 2020, and Dec. 31st, 2020.

additional government regulations on Dec. 16, 2020 [38]. For reference, we indicated this date by the dotted black line in Fig. 1. However, GRs are not explicitly captured by our model. While GRs are also typically in response to higher values of $c(t)$, their switch-like effect on $\Delta_m^{\text{obs}}(t)$ cannot be captured by our continuous model without significant extensions that would also introduce a number of new parameters.

Therefore, the observation that our model can reproduce the initial mobility change much better than at later points in time motivates the hypothesis that the role of voluntary protection behavior (VPB) is more relevant during the onset of the pandemic compared to when individuals are already used to it. Note that this fits well with our model assumption that the perceived severity/susceptibility reduces over time.

4. Coupled Behavior-Disease Model: Introduction and Scenarios

Because our model proved useful to explain mobility change, which can be assumed as a proxy for behavior change, we go one step further and couple $p(t)$ with a model for disease spread.

Note that we do not attempt to fit the resulting infection dynamics to the reported number of cases in some country for two reasons. First, the reported number of cases are subject to a - generally time-varying - undercounting factor which would make the fitting procedure useless. Secondly, even if the true number of infections

were known, or estimated, e.g., using publicly available models like [39], many factors besides a single behavior influence the infection dynamics, like, seasonality [29], hygiene measures [40], or individuals who might adopt different PBs at different prevalences or depending on their vaccination status [5]. Also, mask-wearing, which has been shown to reduce the risk of infection considerably [41], has not been recommended or adopted initially. Only over time, recommendations were changed and both voluntary and government-mandated usage increased.

Therefore, we do not attempt to validate the coupled model with any real-world data. Instead, we present some examples of the complex infection dynamics it can create and provide a comprehensive mathematical analysis of its long-term behavior.

4.1. Model Definition

We use a modified SIR model. Here, the population is divided into three compartments of susceptible, infectious, and recovered individuals, whose sizes are indicated by $s(t)$, $i(t)$, and $r(t)$, respectively. To facilitate theoretical analysis, we assume a normalized population, i.e., $s(t) + i(t) + r(t) = 1 \forall t$.

First, we note that the SIR model can be re-written in

terms of the effective reproduction number $R(t)$, i.e.,

$$\frac{ds(t)}{dt} = -\frac{R(t)}{\tau}i(t) \quad (4)$$

$$\frac{di(t)}{dt} = +\frac{R(t)}{\tau}i(t) - \frac{1}{\tau}i(t) \quad (5)$$

$$\frac{dr(t)}{dt} = +\frac{1}{\tau}i(t), \quad (6)$$

where τ denotes the average duration of infectiousness. In the standard SIR model, $R(t)$ is given by

$$R(t) = R_0 \cdot s(t), \quad (7)$$

where R_0 denotes the basic reproduction number. Now, if we have a hypothesis of how certain actions influence $R(t)$, this formulation gives us a straight-forward way to include them into an SIR model.

In the remainder of this paper, we assume that an increase of $p(t)$ reduces the reproduction number. Specifically, if $p(t) = 0$, we should obtain the same result as for the standard SIR model. But if $p(t) = 1$, we should obtain $R(t) = 0$. Therefore, we use

$$R(t) = R_0 s(t)[1 - p(t)] \quad (8)$$

to couple our behavior model with the infection dynamics. The full model is thus given by

$$\frac{ds(t)}{dt} = -\frac{R_0 s(t)[1 - p(t)]}{\tau}i(t) \quad (9)$$

$$\frac{di(t)}{dt} = +\frac{R_0 s(t)[1 - p(t)]}{\tau}i(t) - \frac{1}{\tau}i(t) \quad (10)$$

$$\frac{dr(t)}{dt} = +\frac{1}{\tau}i(t) \quad (11)$$

$$\frac{dp(t)}{dt} = [f_0 (t + 1)^a i(t)] \cdot [1 - p(t)] - g_0 \cdot p(t) \quad (12)$$

if we use $i(t) = c(t)$.

4.2. Examples of Complex Dynamics

As a first step, we present some examples of the complex dynamics that can be created by our model. Four scenarios are shown in Fig. 2, with the corresponding parameters reported in Appendix C.1. Here, $i(t)$, $r(t)$, and $p(t)$ are shown by the solid pink, green, and turquoise lines, respectively. For reference, we also show the fraction of recovered individuals that would be obtained in the standard SIR model, $r^{\text{SIR}}(t)$, by the dashed green line.

The first scenario is rather similar to the standard SIR model with a single big wave of infections. Here, $p(t)$ increases too slowly to stop the infections. Yet, through comparison of $r(t)$ and $r^{\text{SIR}}(t)$ we can see that the adoption of PB still reduces the prevalence, s.t., the total number of infected individuals is much lower compared to the case without any PB.

In the second scenario, multiple waves of infections occur. There is a very fast initial increase of $p(t)$ which

keeps the first wave extremely low. But over time, $p(t)$ goes down again which enables the emergence of a second wave that is stopped by an increase of $p(t)$ in response to the higher infection levels. Later, $p(t)$ goes down again and causes the emergence of a third wave of infections. After that, $p(t)$ reduces further. However, now, a considerable amount of population immunity has built up, s.t., the peak heights of the waves reduce again.

The third scenario is another one with multiple waves of infection. Similar to the previous scenario, there is a very steep increase of $p(t)$ in the beginning. Again, the peak height of infection waves is determined by the interplay between PB and population immunity.

The fourth scenario is significantly different from the other three as an initial peak value is followed - after dampened oscillations - by approximately constant values of $p(t)$ and $i(t)$.

5. Coupled Behavior-Disease Model: Analysis

Now that we have seen the wide variety of infection dynamics resulting from time-variant risk perception, we provide some analytical insights into the model dynamics.

First, we look at (12) and note that for $a < 0$ we have $f_0 (t + 1)^a i(t) = 0$ for $t \rightarrow \infty$ because $i(t)$ can be bounded from above by some constant i^{max} , e.g., $i^{\text{max}} = 1$. Therefore, for any $g_0 > 0$, we have $p(t) = 0$ for $t \rightarrow \infty$. By looking at (9)-(11), we see that $i(t) = 0$ has to hold, s.t., $s(t)$, $i(t)$, and $r(t)$ do not change anymore.

From this, we know the fate of our model for $t \rightarrow \infty$: Eventually nobody will adopt PB anymore and there won't be any infections³. However, how long it takes to reach this state and the final values of $s(t)$ and $r(t)$ are generally unknown.

5.1. (Approximate) Fixed Point in the Low-Infection Limit

If $R(t) \approx 1$ and $i(t)$ is very small, it can take a very long time until this final state is reached. In fact, it can happen that $r(t)$ increases slow enough such that population immunity has no relevant effect for a very long time. In this case, one can approximate $s(t) \approx 1$. If additionally $a \approx 0$, i.e., the risk-awareness is almost time-invariant, the model dynamics are approximately captured by

$$\frac{di(t)}{dt} = \frac{R_0[1 - p(t)]}{\tau}i(t) - \frac{1}{\tau}i(t) \quad (13)$$

$$\frac{dp(t)}{dt} = f_0 i(t) \cdot [1 - p(t)] - g_0 \cdot p(t). \quad (14)$$

In this setting, $i(t)$ and $p(t)$ are, for large values of t , almost constant and given by

$$i_\infty = \frac{g_0}{f_0}(R_0 - 1) \quad (15)$$

³However, even in models where re-infections are possible, like in the SIRS model, nobody would adopt PB for $t \rightarrow \infty$ if $a < 0$.

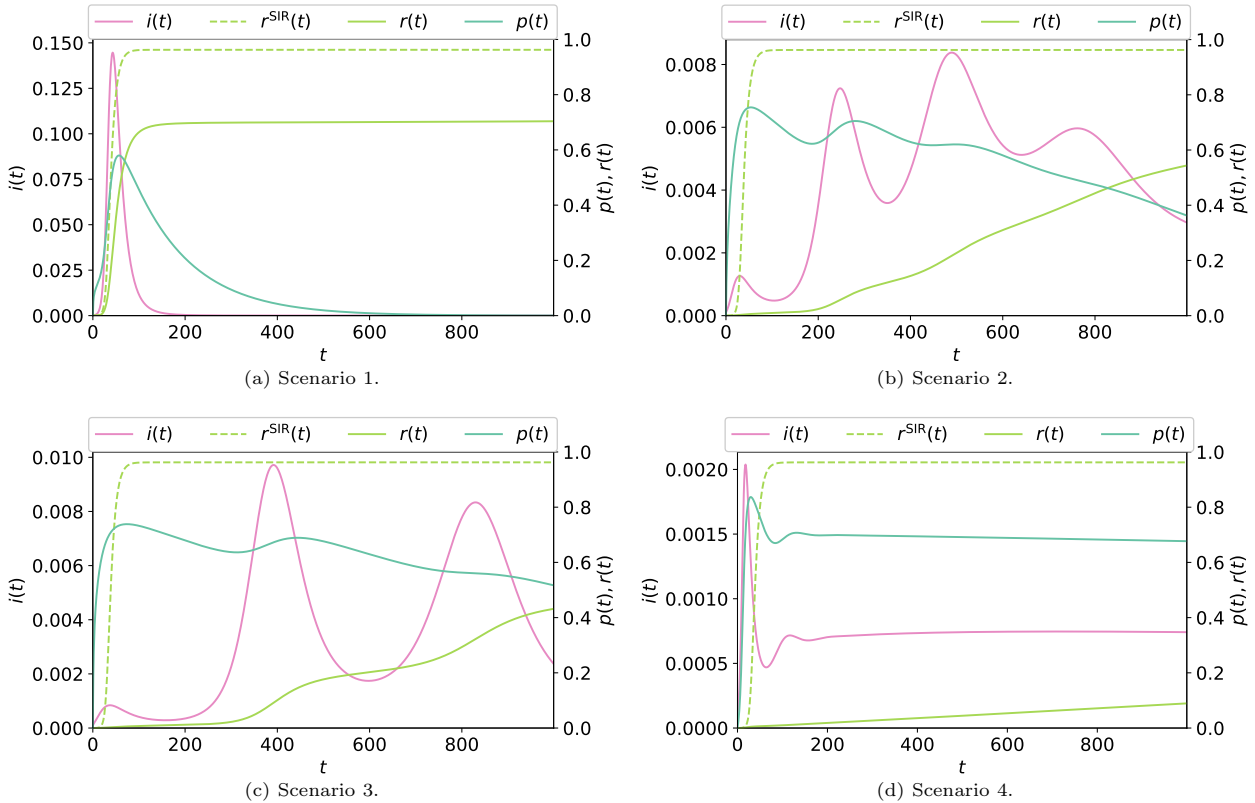


Figure 2: Four scenarios with the fraction of infected individuals (solid purple line), the fraction of individuals adopting PB (solid turquoise line), and the fraction of recovered individuals (solid green line) for different behavior parameters. For reference, the fraction of recovered individuals over time in absence of any PB (dashed green line).

and

$$p_{\infty} = 1 - \frac{1}{R_0}, \quad (16)$$

respectively. For the full derivation and stability analysis, we refer to Appendix D.2. If we use the same parameters as for Scenario 4, we obtain $i_{\infty} \approx 4.3 \cdot 10^{-4}$ and $p_{\infty} \approx 0.7$. These values are indeed of the same order of magnitude as the actual values of $i(t)$ and $p(t)$ that are displayed in Fig. 2d.

5.2. Regimes for Long-Term Infection Dynamics

Generally $a \neq 0$ and $i(t)$ can become large enough such that the previous analysis of the low-infection limit is not valid. Also, as we have shown in Fig. 2, the full behavior-disease model can produce a wide variety of infection dynamics that are hard to predict and understand analytically.

However, the final value of susceptibles $s(\infty)$ might be more predictable. Motivated by this, we plot $s(\infty)$ over $\log_{10}(f_0)$ for different values of g_0 in Fig. 3. The corresponding simulation parameters are reported in Appendix C.2.

One can distinguish two regimes for the final number of susceptibles: For smaller values of f_0 , $s(\infty) \approx s^{\text{SIR}}_{\infty} \approx 0.04$ and for large values of f_0 , $s(\infty) \approx \frac{1}{3.4} \approx 0.3$. In-between there is a transition between these regimes. First, we explain these values and show how the regime can be

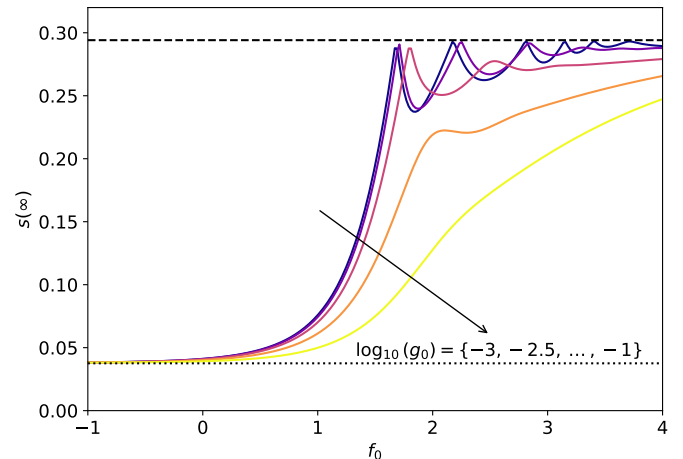


Figure 3: The fraction of susceptible individuals after $t = 5 \cdot 10^4$ days as a function of f_0 . The results are reported for different values of $\log_{10}(g_0)$ which are indicated by increasingly bright colors as $\log_{10}(g_0)$ increases.

predicted based on the initial model dynamics. Finally, we explain the non-smooth dynamics that can be observed for smaller values of g_0 .

5.2.1. Explaining the Regime Values

As described earlier, for any $a < 0$, $p(t)$ will eventually be zero. Therefore, only population immunity can bring $R(t)$ below one in order to exhaust the epidemic. The necessary condition for $R(t) < 1$, if $p(t) = 0$, is

$$s(t) < \frac{1}{R_0}. \quad (17)$$

This upper bound for $s(\infty)$ can be only achieved if $i(t)$ stays small. To illustrate this, consider a wave of infections where $i(t)$ has become large, e.g., $i(t) \approx \frac{1}{5}$. Now, even if $R(t) < 1$ due to population immunity, the wave has still *momentum*, i.e., many more individuals are still getting infected even though the reproduction number is below one.

This is exactly what happens in the standard SIR model without PB. Indeed, for smaller values of f_0 , $s(\infty) \approx s^{\text{SIR}}(\infty)$, where $s^{\text{SIR}}(\infty)$ denotes the final number of susceptibles in the standard SIR model. For reference, we plotted this as the dotted black line in Fig. 3. Indeed, this is the value of the regime with fewer final susceptibles.

On the other hand, if $i(t) \approx 0$, $s(\infty)$ can actually reach the upper bound of $\frac{1}{R_0}$. For reference, we plotted this as the dashed black line in Fig. 3. Indeed, this is the value of the regime with more final susceptibles.

5.2.2. Predicting the Regime for Long-Term Infection Dynamics

Let us check if we can predict in which regime one ends up for given behavior and disease parameters without running the full simulations.

To this end, we ask whether $p(t)$ is large enough, s.t., PB can significantly decrease $R(t)$ before too many individuals got infected in the first wave. First, we observe that $i(t)$ can be approximated for $t \rightarrow 0$, i.e., when $p(t) \approx 0$ and $s(t) \approx 1$ by

$$i(t) \approx i_0 \exp\left(\frac{R_0 - 1}{\tau} t\right) = i_0 \exp(\lambda_0 t), \quad (18)$$

where $i_0 = i(0)$. Similarly, we simplify (12) by assuming $g_0 \approx 0$ and $p(t) \approx 0$ for $t \rightarrow 0$. In this case, $\frac{dp(t)}{dt}$ depends only on t and $i(t)$. Thus, if we have a closed-form expression for $i(t)$ like our approximation in (18), we can obtain $p(t)$ by solving the integral

$$p(t) = \int f_0 i(t) (t+1)^a dt \quad (19)$$

with the initial condition $p(0) = p_0$.

Then, we can ask whether $i(t)$ would reach a value $i_* > 0$ before or after PB has a relevant effect, i.e., when $p(t)$ reaches some value $p_* = \beta \cdot i_*$ with $\beta \in (0, 1]$.

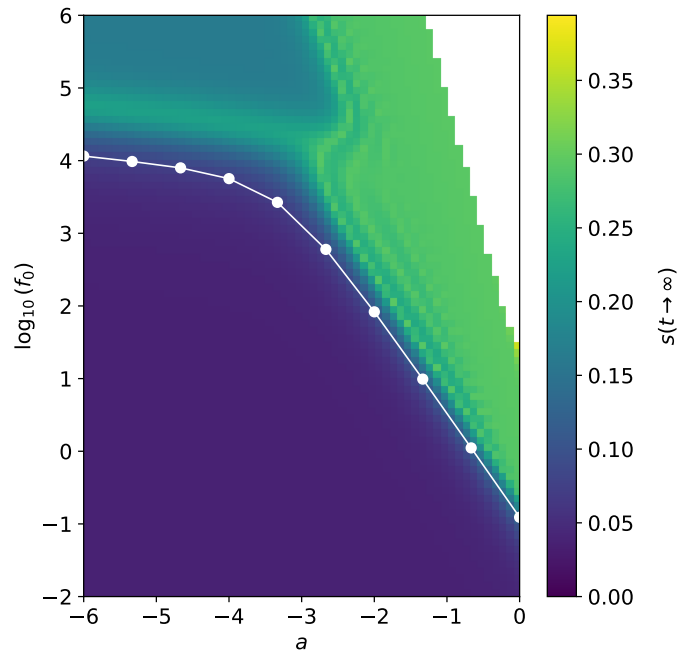


Figure 4: The fraction of susceptible individuals as a function of f_0 and a for exemplary behavior and disease parameters after $t = 5 \cdot 10^4$ days. We indicated the approximated transition between both regime values by the solid white line. The white area indicates parameter combinations where the simulations have not yet converged after $5 \cdot 10^4$ days.

To validate this idea, we run simulations for different values of $\log_{10}(f_0)$ and a with parameters as described in Appendix C.3. We then compute the curve in the a - f_0 -plane where $p(t)$ reaches $p_* = \frac{1}{2} i_* = \frac{1}{4}$ at the same time as $i(t)$ reaches $i_* = \frac{1}{2}$. The procedure to obtain this curve and additional sensitivity analyses are reported in Appendix D.1. In Fig. 4, we indicate $s(\infty)$ by the color and draw the obtained critical curve in white.

For large values of $\log_{10}(f_0)$ and small values of a , the simulations might take an extremely long time to converge. For example, for $a = 0$ and $\log_{10}(f_0) = 5$, the low-infection limit holds and we would obtain $i_\infty = \frac{10^{-2.5}}{10^5} (3.4 - 1) \approx 10^{-7}$, i.e., approximately 10^7 time steps would be necessary until all individuals got infected. In order to reduce the computational load, we use $t_{\text{sim}} = 5 \cdot 10^4$ time steps and do not report $s(t_{\text{sim}}) \approx s(\infty)$ if $i(t_{\text{sim}}) > \frac{1}{10} \cdot i_\infty$.

One can clearly distinguish the two regimes in the parameter space. If $\log_{10}(f_0)$ is large and $|a|$ is small, $s(\infty) \approx \frac{1}{R_0}$, while $s(\infty) \approx s^{\text{SIR}}(\infty)$ if $\log_{10}(f_0)$ is small and $|a|$ is large. The border between both regimes is predicted remarkably well by our approach. Analyzing whether $p(t)$ has a significant effect in the beginning enables interestingly enough insights about the long-term behavior of $s(t)$.

5.2.3. Explaining the Non-Smooth Dependency on f_0

As a final contribution of this paper, we look at the non-smooth dependency of $s(\infty)$ on f_0 that can be observed

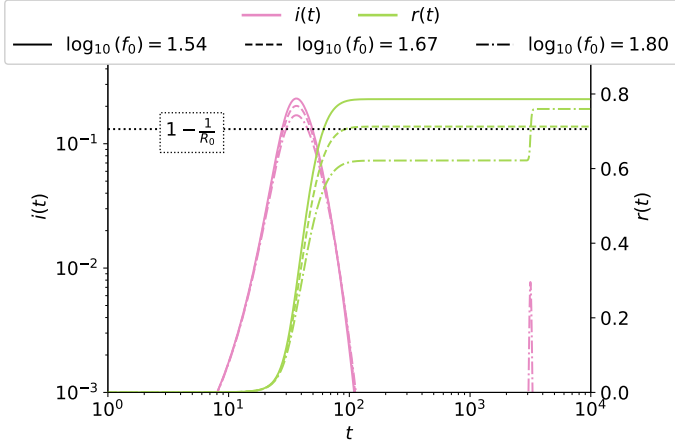


Figure 5: The fraction of infected (purple) and recovered (green) individuals for scenarios with different f_0 . The non-monotonous behavior in Fig. 4 can be explained by the emergence of a second wave.

in Fig. 3. This is a surprising behavior because we would expect that a higher risk perception enables more individuals to escape infection. While this would be true for time-invariant perception, i.e., $a = 0$, the time-dependency causes more complex dynamics.

Indeed, as f_0 increases, the (initial) peak height of infections decreases and fewer people get infected in the first wave. However, if f_0 increases further, a small second wave can emerge, if fewer than $1 - \frac{1}{R_0}$ individuals got infected in the first wave, causing $s(\infty) \ll \frac{1}{R_0}$.

We illustrate this by plotting the time-evolution of $i(t)$ and $r(t)$ for $\log_{10}(f_0) \in \{1.54, 1.67, 1.80\}$ in Fig. 5 with the same parameters as used for Fig. 3 with $\log_{10}(g_0) = -3.0$. Indeed, the peak height of the first wave reduces with increasing values of $\log_{10}(f_0)$ but for $\log_{10}(f_0) = 1.80$, a second wave can emerge causing more overall infections compared to the scenario with $\log_{10}(f_0) = 1.67$. We also plotted $1 - \frac{1}{R_0}$ into Fig. 5, s.t., we can compare $r(t)$ to the critical value for which population immunity prevents $R(t) > 1$. Indeed, only in the scenario with $\log_{10}(f_0) = 1.80$, enough susceptibles are left after the first wave to cause a second wave.

6. Conclusion

In this paper, we proposed a simple model to describe the behavioral response to the outbreak of an emerging disease. Our model is motivated by the Health Belief Model, a commonly used concept from health psychology that assumes that the adoption of protection behavior depends on the perceived severity of a disease and the perceived likelihood of infection. Therefore, individuals adopt protection behavior in response to the reported disease prevalence in our model. However, over time the perceived risk associated with the reported prevalence goes down.

We validated the proposed behavior model with real-world mobility data during the COVID-19 pandemic in

2020. Despite its simplicity and its lack of explicit consideration of government regulations, the major trends of the observed mobility reduction are reproduced for different European countries. This indicates that time-varying risk perception facilitates understanding the behavioral response to the outbreak of a novel disease over long periods of time.

Additionally, we analyzed what happens if the behavior model is coupled with an susceptible-infectious-removed model for infection dynamics. We demonstrate the emergence of complex dynamics, including multiple waves of infections. We identified two regimes for the final number of susceptibles: one regime with similar values to the default susceptible-infectious-removed model and the other with similar values close to $\frac{1}{R_0}$, where R_0 is the basic reproduction number. Through detailed analysis, we derived a bound to predict the transition between both regimes depending on whether the adoption of protection behavior is fast enough.

Finally, we observed that the model exhibits a non-monotonous relationship of increasing risk-perception and the final number of susceptibles. This can be explained through the emergence of subsequent infection waves as a consequence of the complex interplay of protection behavior, population immunity, and changes in risk-perception over time.

In future work, one could extend the behavior model to incorporate government regulations and other factors like the availability of vaccines or the emergence of variants of concern. This could enable an improved model fit over longer time-frames. Furthermore, one could incorporate the behavior model in a more realistic model for disease spread that captures, e.g., the possibility of re-infections or non-homogenous mixing of different population groups.

Acknowledgement

Bastian Heinlein would like to thank Reinhard German and Anatoli Djanatliev for their support to enable his research stay with Manlio De Domenico. Furthermore, he would like to thank Timo Jakumeit and Hannah Stephan for their valuable comments on the manuscript.

References

- [1] J. Wise, Covid-19: Who declares end of global health emergency (2023).
- [2] A. Collis, K. Garimella, A. Moehring, M. A. Rahimian, S. Babalola, N. H. Gobat, D. Shattuck, J. Stolow, S. Aral, D. Eckles, Global survey on covid-19 beliefs, behaviours and norms, *Nature Human Behaviour* 6 (9) (2022) 1310–1317.
- [3] C. Betsch, L. H. Wieler, K. Habersaat, Monitoring behavioural insights related to covid-19, *The Lancet* 395 (10232) (2020) 1255–1256.
- [4] A. Koher, F. Jørgensen, M. B. Petersen, S. Lehmann, Epidemic modelling of monitoring public behavior using surveys during pandemic-induced lockdowns, *Communications Medicine* 3 (1) (2023) 80. doi:10.1038/s43856-023-00310-z.

- [5] J. Wambua, N. Loedy, C. I. Jarvis, K. L. Wong, C. Faes, R. Grah, B. Prasse, F. Sandmann, R. Niehus, H. Johnson, et al., The influence of covid-19 risk perception and vaccination status on the number of social contacts across europe: insights from the comix study, *BMC Public Health* 23 (1) (2023) 1–13.
- [6] Google LLC, Google covid-19 community mobility reports. URL <https://www.google.com/covid19/mobility/>
- [7] Apple, Covid-19 mobility trends reports. URL <https://covid19.apple.com/mobility>
- [8] T. L. Webb, P. Sheeran, Does changing behavioral intentions engender behavior change? a meta-analysis of the experimental evidence., *Psychological bulletin* 132 (2) (2006) 249.
- [9] L. Hufnagel, D. Brockmann, T. Geisel, Forecast and control of epidemics in a globalized world, *Proceedings of the national academy of sciences* 101 (42) (2004) 15124–15129.
- [10] H. S. Badr, H. Du, M. Marshall, E. Dong, M. M. Squire, L. M. Gardner, Association between mobility patterns and covid-19 transmission in the usa: a mathematical modelling study, *The Lancet Infectious Diseases* 20 (11) (2020) 1247–1254.
- [11] P. Nouvellet, S. Bhatia, A. Cori, K. E. Ainslie, M. Baguelin, S. Bhatt, A. Boonyasiri, N. F. Brazeau, L. Cattarino, L. V. Cooper, et al., Reduction in mobility and covid-19 transmission, *Nature communications* 12 (1) (2021) 1090.
- [12] S. Jewell, J. Futoma, L. Hannah, A. C. Miller, N. J. Foti, E. B. Fox, It’s complicated: characterizing the time-varying relationship between cell phone mobility and covid-19 spread in the us, *NPJ digital medicine* 4 (1) (2021) 152.
- [13] F. Delussu, M. Tizzoni, L. Gauvin, The limits of human mobility traces to predict the spread of covid-19: A transfer entropy approach, *PNAS Nexus* (2023) pgad302arXiv:<https://academic.oup.com/pnasnexus/advance-article-pdf/doi/10.1093/pnasnexus/pgad302/51552116/pgad302.pdf>, doi:10.1093/pnasnexus/pgad302. URL <https://doi.org/10.1093/pnasnexus/pgad302>
- [14] F. Schlosser, B. F. Maier, O. Jack, D. Hinrichs, A. Zachariae, D. Brockmann, Covid-19 lockdown induces disease-mitigating structural changes in mobility networks, *Proceedings of the National Academy of Sciences* 117 (52) (2020) 32883–32890.
- [15] B. T. Snoeijer, M. Burger, S. Sun, R. J. Dobson, A. A. Folarin, Measuring the effect of non-pharmaceutical interventions (npis) on mobility during the covid-19 pandemic using global mobility data, *NPJ digital medicine* 4 (1) (2021) 81.
- [16] N. Askitas, K. Tatsiramos, B. Verheyden, Estimating worldwide effects of non-pharmaceutical interventions on covid-19 incidence and population mobility patterns using a multiple-event study, *Scientific reports* 11 (1) (2021) 1972.
- [17] G. Pullano, E. Valdano, N. Scarpa, S. Rubrichi, V. Colizza, Evaluating the effect of demographic factors, socioeconomic factors, and risk aversion on mobility during the covid-19 epidemic in france under lockdown: a population-based study, *The Lancet Digital Health* 2 (12) (2020) e638–e649.
- [18] C. Santana, F. Botta, H. Barbosa, F. Privitera, R. Menezes, R. Di Clemente, Covid-19 is linked to changes in the time–space dimension of human mobility, *Nature Human Behaviour* (2023) 1–11.
- [19] S. Funk, M. Salathé, V. A. Jansen, Modelling the influence of human behaviour on the spread of infectious diseases: a review, *Journal of the Royal Society Interface* 7 (50) (2010) 1247–1256.
- [20] N. Perra, D. Balcan, B. Gonçalves, A. Vespignani, Towards a characterization of behavior-disease models, *PloS one* 6 (8) (2011) e23084.
- [21] M. Ye, L. Zino, A. Rizzo, M. Cao, Game-theoretic modeling of collective decision making during epidemics, *Physical Review E* 104 (2) (2021) 024314.
- [22] B. Morsky, F. Magpantay, T. Day, E. Akçay, The impact of threshold decision mechanisms of collective behavior on disease spread, *Proceedings of the National Academy of Sciences* 120 (19) (2023) e2221479120.
- [23] M. Soltanolkottabi, D. Ben-Arieh, C.-H. Wu, Modeling behavioral response to vaccination using public goods game, *IEEE transactions on computational social systems* 6 (2) (2019) 268–276.
- [24] M. A. Amaral, M. M. de Oliveira, M. A. Javarone, An epidemiological model with voluntary quarantine strategies governed by evolutionary game dynamics, *Chaos, Solitons & Fractals* 143 (2021) 110616.
- [25] S. Kim, Y. B. Seo, E. Jung, Prediction of covid-19 transmission dynamics using a mathematical model considering behavior changes in korea, *Epidemiology and health* 42 (2020).
- [26] T. Usherwood, Z. LaJoie, V. Srivastava, A model and predictions for covid-19 considering population behavior and vaccination, *Scientific reports* 11 (1) (2021) 12051.
- [27] D. P. Durham, E. A. Casman, Incorporating individual health-protective decisions into disease transmission models: a mathematical framework, *Journal of the Royal Society Interface* 9 (68) (2012) 562–570.
- [28] Y. Ge, W.-B. Zhang, X. Wu, C. W. Ruktanonchai, H. Liu, J. Wang, Y. Song, M. Liu, W. Yan, J. Yang, et al., Untangling the changing impact of non-pharmaceutical interventions and vaccination on european covid-19 trajectories, *Nature Communications* 13 (1) (2022) 3106.
- [29] T. Gavenčiak, J. T. Monrad, G. Leech, M. Sharma, S. Mindermann, S. Bhatt, J. Brauner, J. Kulveit, Seasonal variation in sars-cov-2 transmission in temperate climates: A bayesian modelling study in 143 european regions, *PLoS Computational Biology* 18 (8) (2022) e1010435.
- [30] E. C. Green, E. M. Murphy, K. Gryboski, The health belief model, *The Wiley encyclopedia of health psychology* (2020) 211–214.
- [31] P. Poletti, M. Ajelli, S. Merler, The effect of risk perception on the 2009 h1n1 pandemic influenza dynamics, *PloS one* 6 (2) (2011) e16460.
- [32] P. Barbrook-Johnson, J. Badham, N. Gilbert, Uses of agent-based modeling for health communication: The tell me case study, *Health Communication* 32 (8) (2017) 939–944.
- [33] A. Bish, S. Michie, Demographic and attitudinal determinants of protective behaviours during a pandemic: A review, *British journal of health psychology* 15 (4) (2010) 797–824.
- [34] M. Scopelliti, M. G. Pacilli, A. Aquino, Tv news and covid-19: Media influence on healthy behavior in public spaces, *International journal of environmental research and public health* 18 (4) (2021) 1879.
- [35] C. Muñiz, Media system dependency and change in risk perception during the covid-19 pandemic (2020).
- [36] I. Pilch, P. Wardawy, E. Proberz, The predictors of adaptive and maladaptive coping behavior during the covid-19 pandemic: The protection motivation theory and the big five personality traits, *PLoS One* 16 (10) (2021) e0258606.
- [37] S. Shiloh, S. Peleg, G. Nudelman, Adherence to covid-19 protective behaviors: A matter of cognition or emotion?, *Health Psychology* 40 (7) (2021) 419.
- [38] N. Perumal, A. Steffen, A. Ullrich, A. Siedler, Impact of covid-19 immunisation on covid-19 incidence, hospitalisations, and deaths by age group in germany from december 2020 to october 2021, *Vaccine* 40 (21) (2022) 2910–2914.
- [39] Institute for Health Metrics and Evaluation, Covid-19 projections. URL <https://covid19.healthdata.org/projections>
- [40] D. Gursoy, C. G. Chi, Effects of covid-19 pandemic on hospitality industry: review of the current situations and a research agenda, *Journal of Hospitality Marketing & Management* 29 (5) (2020) 527–529. doi:10.1080/19368623.2020.1788231.
- [41] G. Bagheri, B. Thiede, B. Hejazi, O. Schlenzcek, E. Bodenschatz, An upper bound on one-to-one exposure to infectious human respiratory particles, *Proceedings of the National Academy of Sciences* 118 (49) (2021) e2110117118.
- [42] E. Mathieu, H. Ritchie, L. Rodés-Guirao, C. Appel, C. Giattino, J. Hasell, B. Macdonald, S. Dattani, D. Beltekian, E. Ortiz-Ospina, M. Roser, Coronavirus pandemic (covid-19), *Our World in Data* <https://ourworldindata.org/coronavirus> (2020).
- [43] P. Virtanen, R. Gommers, T. E. Oliphant, M. Haberland, T. Reddy, D. Cournapeau, E. Burovski, P. Peterson,

W. Weckesser, J. Bright, et al., Scipy 1.0: fundamental algorithms for scientific computing in python, *Nature methods* 17 (3) (2020) 261–272.

- [44] M. Newville, T. Stensitzki, D. B. Allen, M. Rawlik, A. Ingargiola, A. Nelson, Lmfit: Non-linear least-square minimization and curve-fitting for python, *Astrophysics Source Code Library* (2016) ascl-1606.
- [45] R. Storn, K. Price, Differential evolution—a simple and efficient heuristic for global optimization over continuous spaces, *Journal of global optimization* 11 (1997) 341–359.
- [46] J. Dehning, J. Zierenberg, F. P. Spitzner, M. Wibral, J. P. Neto, M. Wilczek, V. Priesemann, Inferring change points in the spread of covid-19 reveals the effectiveness of interventions, *Science* 369 (6500) (2020) eabb9789.

Appendix A. Behavior Model Validation: Data Sources and Methods

Appendix A.1. Data Sources

To validate our behavior model, we use the smoothed number of reported cases per 100,000 inhabitants provided by Our World in Data (OWID) [42] as $c(t)$. As additional pre-processing we normalize these values such that $c(t)$ has unit variance between Mar. 1st, 2020 and Feb. 01st, 2021.

We use aggregate mobility data on a country level for the category *retail and recreation* as reported by Google [6]. In these data, daily mobility change relative to a pre-pandemic baseline is given. However, because the raw data is subject to strong periodic weekly fluctuations, we convolve the data with a finite impulse response (FIR) filter with impulse response $h(t) = \frac{1}{7} \sum_{\tau=0}^6 \delta(t - \tau)$, where $\delta(\cdot)$ is the Delta-Dirac function.

Appendix A.2. ODE Simulations

Note that we have only discrete-time data $c^{\text{discrete}}[k]$, $k \in \mathbb{Z}$ with a resolution on a daily level, but ODEs, i.e., a continuous simulation method. Therefore, we use

$$c(t) = c^{\text{discrete}}[\lfloor t \rfloor], \quad (\text{A.1})$$

where $\lfloor \cdot \rfloor$ denotes the floor function. Comparing $p(t)$ to mobility data is straight-forward because we can sample $p(t)$ at non-negative integer values of t .

The ODEs are simulated using the RK45 method of *scipy* [43] with $\text{atol} = 10^{-6}$ and $\text{rtol} = 10^{-3}$.

Appendix A.3. Parameter Fitting

We use $p(0) = \max\{0, -\Delta_m^{\text{obs}}(0)\}$ as initial condition. For the fitting procedure, we use only negative values for the mobility change, i.e., we compare $p(t)$ to $\text{ReLU}(-\Delta_m^{\text{obs}}(t))$ because our mobility model assumes that $m^{\text{obs}}(t) = m^{\text{base}} \cdot [1 - p(t)]$ and thus can only model mobility decrease.

We use the *lmfit* wrapper [44] around the *scipy* [43] implementation of differential evolution [45] to solve the optimization problem of finding $\log_{10}(f_0) \in [-1, 3]$, $\log_{10}(g_0) \in [-3, 0]$, $a \in [-3, 0]$ that minimize (3).

Parameter	t_{sim}	R_0	τ	i_0	p_0
Value	1000	3.4	8.3	10^{-4}	10^{-4}

Table C.1: Shared parameters used in all scenarios for Fig. 2.

	$\log_{10}(f_0)$	a	$\log_{10}(g_0)$
Scenario 1	3.0	-2.25	-2.10
Scenario 2	3.25	-1.30	-2.55
Scenario 3	3.50	-1.50	-3.00
Scenario 4	2.00	-0.10	-1.75

Table C.2: Scenario-specific parameters used for Fig. 2.

Appendix B. Behavior Model Validation: Sensitivity Analysis

To verify that our behavior model is a robust explanation for mobility change, we performed additional parameter inferences as sensitivity analysis. Specifically, we varied the end date of the considered time period. Otherwise, we use the same simulation and inference procedure as for the default case.

In Fig. B.6, we show the inferred parameters for $\log_{10}(f_0)$, $\log_{10}(g_0)$, and a depending on the chosen time frame. The different countries are indicated by the colors and the different end dates by the marker. For most countries, the inferred parameter values do not change much depending on the end date. Denmark has the largest variations which can be explained by looking at Fig. 1. The second larger mobility reduction happens at the very end of 2020 and thus is not captured by the dataset with Dec. 31st, 2020 as end date. Additionally, the increase of mobility reduction is extremely steep despite the fact that case numbers already increased considerably before. This indicates that the introduction of GRs is an important factor here, as well.

In Fig. B.7, we show the RMSE for each end date and each country. In most countries, the error increases as time increases, probably because the longer the time-frame the more "opportunity" for other factors besides the reported number of cases to influence the population behavior. Overall, we observe that our model inference behaves robustly.

Appendix C. Coupled Behavior-Disease Model: Parameter Values

Appendix C.1. Scenarios

The parameters shared between the four exemplary scenarios are reported in Table C.1. The values for R_0 and τ are taken from [46] in order to resemble values similar to the ones observed in the COVID-19 pandemic before the emergence of variants of concern (VoC). In Table C.2, we report the behavior parameters used for the respective scenarios.

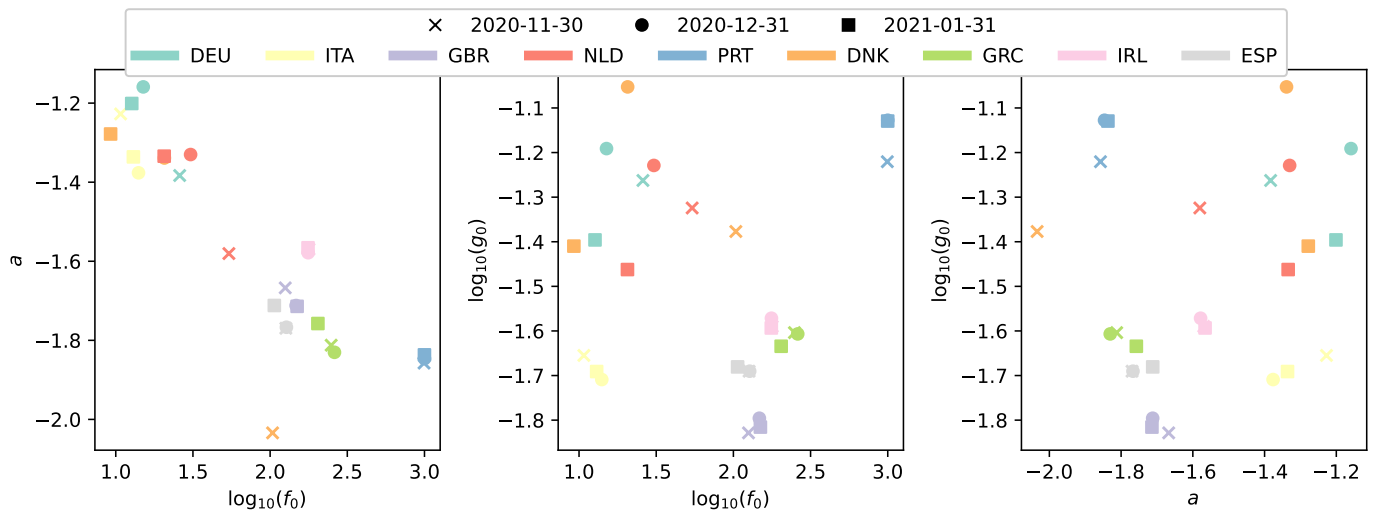


Figure B.6: Best-fitting model parameters for the considered European countries (indicated by color) and varying end dates (indicated by the marker shape).

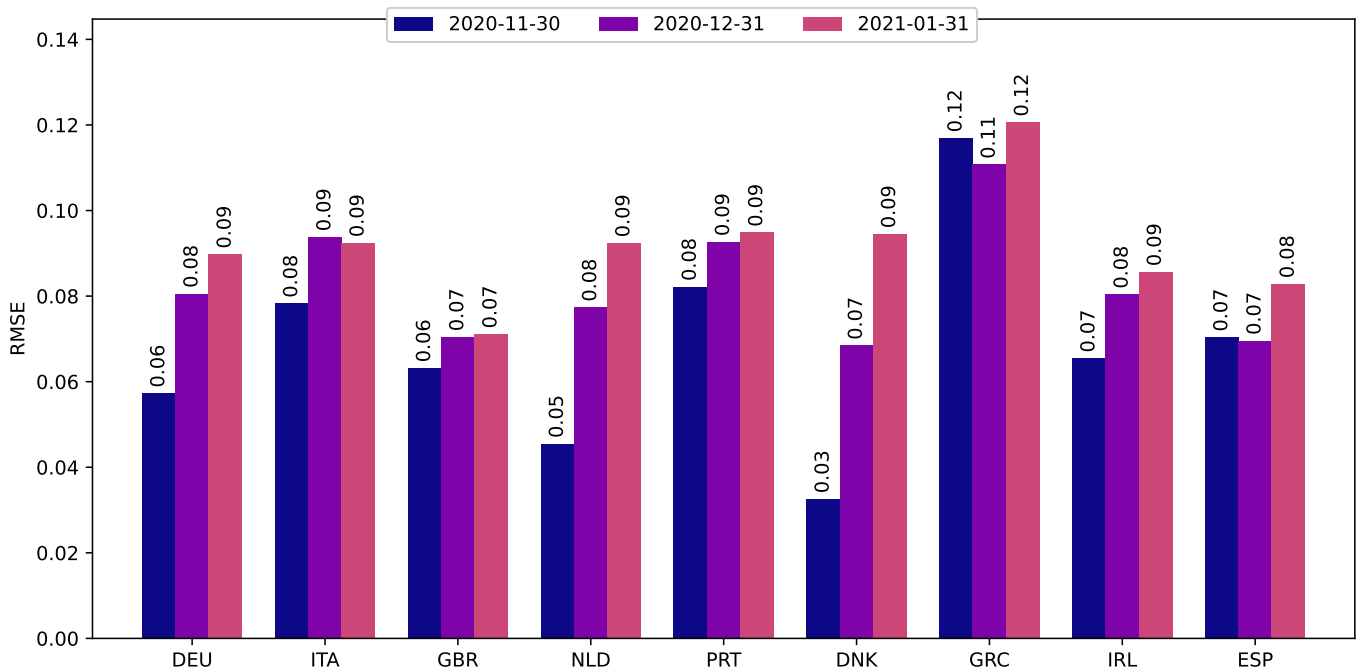


Figure B.7: Errors between the estimated best-fitting model and observed mobility reduction in European countries for different end dates.

Parameter	Meaning	Value
t_{sim}	Simulation Time	$5 \cdot 10^4$
atol	Absolute tolerance for RK45	10^{-20}
rtol	Relative tolerance for RK45	10^{-10}
R_0	Basic Reproduction Number	3.4
τ	Mean Duration of Infectiousness	8.3
i_0	Fraction of initially infected	10^{-4}
p_0	Fraction initially adopting PB	10^{-4}
a	Forgetting Factor	-1.5

Table C.3: Fixed parameter values used to create Fig. 3.

Parameter	Meaning	Value
t_{sim}	Simulation Time	$5 \cdot 10^4$
atol	Absolute tolerance for RK45	10^{-12}
rtol	Relative tolerance for RK45	10^{-6}
R_0	Basic Reproduction Number	3.4
τ	Mean Duration of Infectiousness	8.3
i_0	Fraction of initially infected	10^{-4}
p_0	Fraction initially adopting PB	10^{-4}
$\log_{10}(g_0)$	Tendency to stop adopting PB	-2.5
i_*	-	$\frac{1}{2}$
β	-	$\frac{1}{2}$

Table C.4: Fixed parameter values used to create Fig. 4.

Appendix C.2. Non-Smooth Dependency of $s(\infty)$ on f_0

We show the parameters used to create Fig. 3 in Table C.3. For each curve, we vary $\log_{10}(f_0)$ between -1 and 4 over 250 steps. Each curve corresponds to a value of $\log_{10}(g_0) \in \{-3.0, -2.5, -2.0, -1.5, -1.0\}$.

Appendix C.3. a - f_0 -Plane

We report the fixed simulation parameters for the a - f_0 -plane in Table C.4. For the simulations we vary $\log_{10}(f_0)$ between -2 and 6 over 80 uniformly spaced steps. In the same manner, we vary a between -6 and 0 over 60 uniformly spaced steps.

Appendix D. Coupled Behavior-Disease Model: Full Derivations

Appendix D.1. Regime Bounds

Here, we explain how the critical curve in the a - f_0 -plane can be obtained. First, we observe that the time $t_{i,*}$ at which $i(t) = i_*$ can be obtained as

$$t_{i,*} = \frac{1}{\lambda_0} \log \left(\frac{i_*}{i_0} \right) \quad (\text{D.1})$$

by solving (18) for t .

On the other hand, obtaining the time when $p(t) = p_*$ is more difficult. First, we need an analytical expression for $p(t)$. If we insert (18) into (19), we get

$$p(t) = \int f_0 i_0 e^{\lambda_0 t} (t+1)^a dt, \quad (\text{D.2})$$

for which no closed form integral solution exists to the best of the authors' knowledge. However, we can approximate $p(t)$ by writing $\exp(\lambda_0 t)$ as a Taylor series of n -th order around $t = -1$, i.e.,

$$e^{\lambda_0 t} \approx \sum_{k=0}^n \frac{\lambda_0^k}{k!} e^{-\lambda_0} (t+1)^k. \quad (\text{D.3})$$

This yields

$$p(t) \approx \int f_0 i_0 (t+1)^a \sum_{k=0}^n \frac{\lambda_0^k}{k!} e^{-\lambda_0} (t+1)^k dt + c \quad (\text{D.4})$$

$$= f_0 i_0 e^{-\lambda_0} \sum_{k=0}^n \frac{\lambda_0^k}{k!} \int (t+1)^{a+k} dt + c \quad (\text{D.5})$$

$$= f_0 i_0 e^{-\lambda_0} \sum_{k=0}^n \frac{\lambda_0^k}{k!} \begin{cases} \frac{1}{a+k+1} (t+1)^{a+k+1} & \text{if } a+k \neq -1 \\ \log(1+t) & \text{if } a+k = -1 \end{cases} + c. \quad (\text{D.6})$$

Here, c is a constant ensuring that $p(0) = p_0$.

Algorithm 1 Equation Solver Algorithm

Require: $x_0, f(x), y_*, n_{\text{iterations}}$

```

for  $i = 1, \dots, n_{\text{iterations}}$  do
   $y_i = f(x_{i-1})$ 
  if  $y_i < y_*$  then
     $x_i \leftarrow x_{i-1} + \Delta_x$ 
  else
     $\Delta_x \leftarrow \frac{1}{2} \Delta_x$ 
     $x_i \leftarrow x_{i-1} - \Delta_x$ 
  end if
end for
return  $x_i$ 

```

We cannot expect to find an analytical expression for $t_{p,*}$, i.e, when $p(t) = p_*$. However, we know that $p(t)$ is a monotonously increasing function for $t \geq 0$. Therefore, we can apply Algorithm 1 to find $t_{p,*}$ with $f(t) = p(t)$, $\Delta_x = 10.0$, $x_0 = t_0 = 0.0$, $n_{\text{iterations}} = 20$, and $y_* = p_*$.

To obtain a point on the critical curve in the $f_0 - a$ -plane for a given a , we also use Algorithm 1 but with \geq instead of $<$ in the **if**-condition. However, here $f(x)$ is $t_{p,*}(f_0)$ obtained as described by the previous paragraph. We thus use $x_0 = -2$, $\Delta_x = 1.0$, $n_{\text{iterations}} = 20$, and $y_* = t_{i,*}$.

Appendix D.2. Fixed Point Analysis

Here, we provide more detailed derivations for the fixed point analysis in the low infection regime.

Appendix D.2.1. Determination of the Fixed Point

To compute the fixed point in the low-infection limit, we insert $i(t) = i_\infty$ and $p(t) = p_\infty$ into (13) and (14) and set the resulting equations to zero. First, (13) is solved straight-forwardly for p_∞ . Then, (14) is solved for i_∞ and the previously obtained definition for p_∞ is inserted.

Appendix D.2.2. Fixed Point Stability

To determine whether the obtained fixed point is stable, we first write the ODE system in vector form, i.e.,

$$\mathbf{x} = \begin{bmatrix} \frac{di(t)}{dt} \\ \frac{dp(t)}{dt} \end{bmatrix} = \begin{bmatrix} h_1(p(t), i(t)) \\ h_2(p(t), i(t)) \end{bmatrix}. \quad (\text{D.7})$$

Then, $\mathbf{x}_* = [i_\infty \ p_\infty]^\text{T}$ is a stable fixed point if both eigenvalues of the Jacobian \mathcal{J} evaluated at \mathbf{x}_* have negative real parts. For general values of $i(t) = i$, $p(t) = p$, the Jacobian is given by

$$\mathcal{J} = \begin{bmatrix} \partial_i h_1 & \partial_p h_1 \\ \partial_i h_2 & \partial_p h_2 \end{bmatrix} = \begin{bmatrix} \frac{R_0(1-p)-1}{f_0(1-p)} & -\frac{R_0 i}{\tau} \\ \frac{f_0}{R_0} & -g_0 R_0 \end{bmatrix}. \quad (\text{D.8})$$

If we insert \mathbf{x}_* into \mathcal{J} , we get

$$\mathcal{J}_* = \begin{bmatrix} 0 & \frac{R_0 \frac{g_0}{f_0} (R_0 - 1)}{\tau} \\ \frac{f_0}{R_0} & -g_0 R_0 \end{bmatrix}. \quad (\text{D.9})$$

Then, we can compute the eigenvalues $\mu_{1,2}$ by setting the determinant of \mathcal{J}_* to zero, i.e.,

$$\det(\mathcal{J}) = \begin{vmatrix} 0 - \mu & \frac{R_0 \frac{g_0}{f_0} (R_0 - 1)}{\tau} \\ \frac{f_0}{R_0} & -g_0 R_0 - \mu \end{vmatrix} = 0. \quad (\text{D.10})$$

Multiplying this out, gives a quadratic equation, namely,

$$\mu^2 + (g_0 R_0) \mu + \frac{f_0}{R_0} \cdot \frac{R_0 \frac{g_0}{f_0} (R_0 - 1)}{\tau} = 0, \quad (\text{D.11})$$

which can be solved to

$$\mu_{1/2} = \frac{1}{2} \left(-g_0 R_0 \pm \sqrt{(g_0 R_0)^2 - 4 \cdot \frac{g_0 (R_0 - 1)}{\tau}} \right). \quad (\text{D.12})$$

First, we consider μ_1 :

$$\mu_1 < 0 \quad (\text{D.13})$$

$$\sqrt{(g_0 R_0)^2 - 4 \cdot \frac{g_0 (R_0 - 1)}{\tau}} < g_0 R_0 \quad (\text{D.14})$$

$$(g_0 R_0)^2 - 4 \cdot \frac{g_0 (R_0 - 1)}{\tau} < (g_0 R_0)^2 \quad (\text{D.15})$$

$$-4 \cdot \frac{g_0 (R_0 - 1)}{\tau} < 0. \quad (\text{D.16})$$

Because $R_0 > 1$, $g_0 \geq 0$, and $\tau > 0$, we see that μ_1 is negative for any positive g_0 , i.e., whenever there is at least some tendency to stop adopting PB.

For μ_2 , we differentiate between whether it is real- or complex-valued. If it is real-valued, we know that $\sqrt{\cdot} \leq g_0 R_0$ and thus, μ_2 is negative for any $g_0, R_0 > 0$. If it is complex valued, i.e., the radicand is negative, we have $\Re\{\mu_2\} = -\frac{1}{2}g_0 R_0$. Thus, we can see that the equilibrium is indeed stable for all reasonable parameter values if there is at least some cost associated with PB.

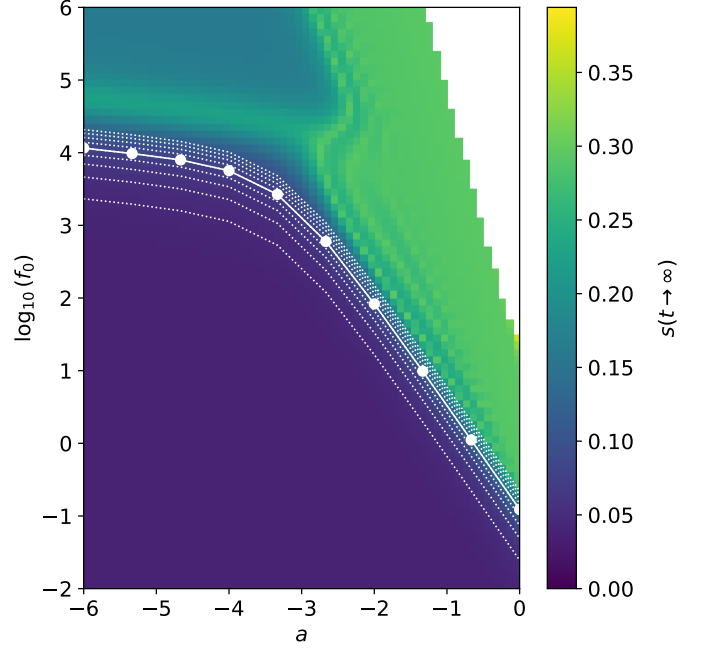


Figure E.8: Sensitivity analysis for Fig. 4 with varied values of β .

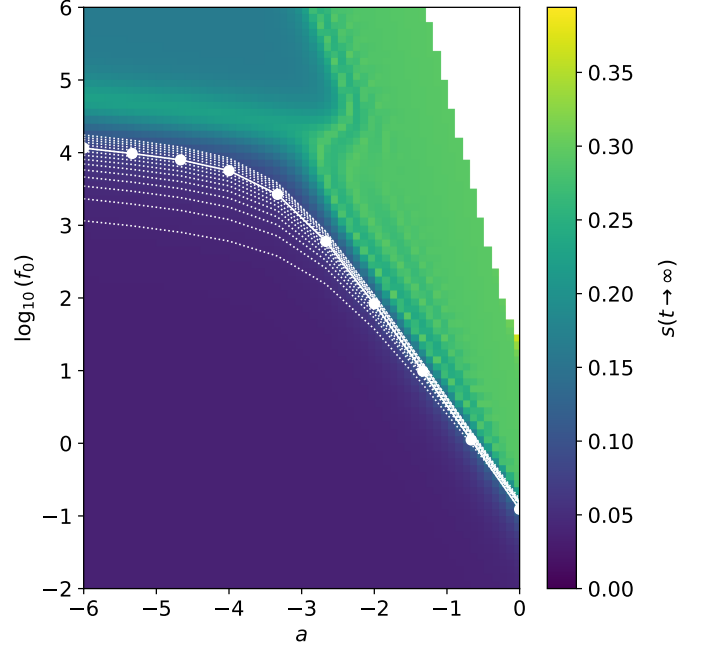


Figure E.9: Sensitivity analysis for Fig. 4 with varied values of i_* .

Appendix E. Coupled Behavior-Disease Model: Sensitivity Analysis

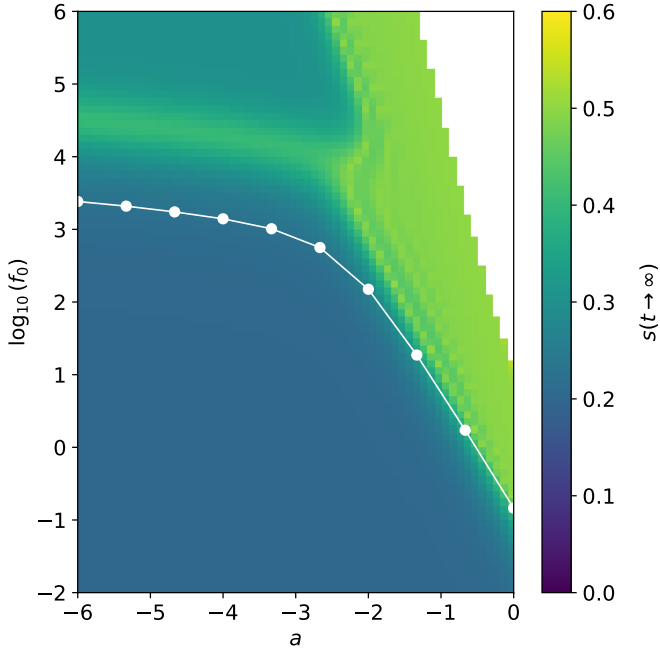


Figure E.10: Sensitivity analysis for Fig. 4 with $R_0 = 2$.

To verify that the critical curve we identified in the a - f_0 -plane is not arbitrary, we provide additional sensitivity analyses here. In Fig. E.8, we take the same parameters as for the plot in the main text, but vary $\beta \in \{0.1, 0.2, \dots, 0.9\}$. In Fig. E.9, we take the same parameters as for the plot in the main text, but vary $i_* \in \{0.05, 0.1, 0.15, \dots, 0.75\}$. We show the curve obtained for the standard values as a reference and the other values by dotted white lines.

In Fig. E.10, we perform the analysis for the same values as for the main plot, but set R_0 to 2. Because fewer individuals will get infected even in absence of any PB, we also reduce i_* to 0.1 to obtain the critical curve.

Finally, in Fig. E.11, we perform the same analysis as in the main plot, but for $\log_{10}(g_0) = -1.0$. In this scenario, our method to obtain the critical curve over-estimates the ability of PB in the first wave to have a lasting effect if a is small. This is because the combination of a fast awareness decay and high cost of PB enables the emergence of a second wave that is essentially not mitigated by PB. Because our method to obtain the critical curve essentially considers only the first wave, these effects cannot be captured.

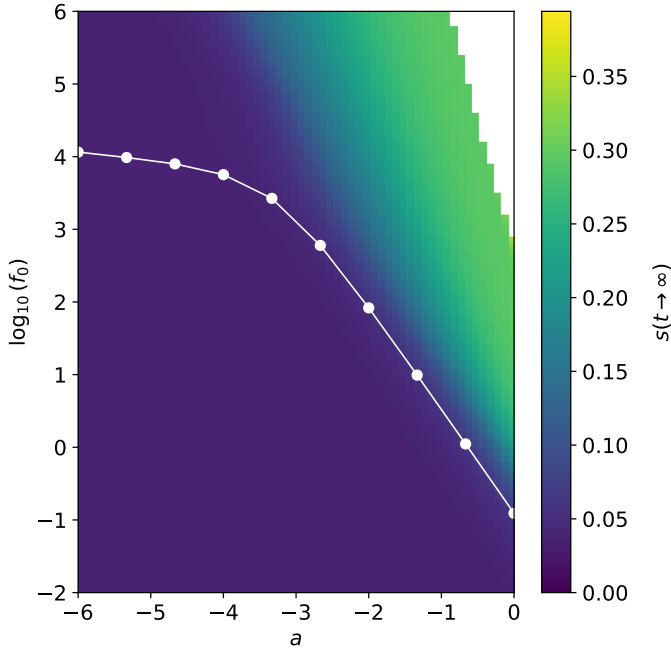


Figure E.11: Sensitivity analysis for Fig. 4 with $\log_{10}(g_0) = -1.0$.